

1 **Energy flux controls tetraether lipid cyclization in *Sulfolobus acidocaldarius***

2

3 Alice Zhou^{1,*}, Beverly K. Chiu¹, Yuki Weber², Felix J. Elling², Alec B. Cobban¹, Ann Pearson²,
4 William D. Leavitt^{1,3,4,*}

5

6 ¹Department of Earth Sciences, Dartmouth College, Hanover, NH 03755

7 ²Department of Earth & Planetary Sciences, Harvard University, Cambridge, MA 02318

8 ³Department of Chemistry, Dartmouth College, Hanover, NH 03755

9 ⁴Department of Biological Sciences, Dartmouth College, Hanover, NH 03755

10 *Correspondence: Alice.Zhou.GR@dartmouth.edu, William.D.Leavitt@dartmouth.edu

11 *Keywords:* archaea, tetraether, ring index, TEX86, chemostat, thermoacidophile

12

13 **Significance Statement**

14 **Microbial lipid membranes protect and isolate a cell from its environment while regulating**
15 **the flow of energy and nutrients to metabolic reaction centers within. We demonstrate that**
16 **membrane lipids change as a function of energy flux using a well-studied archaeon that**
17 **thrives in acidic hot springs and observe an increase in membrane packing as energy**
18 **becomes more limited. These observations are consistent with chemostat experiments**
19 **utilizing a low temperature, neutral pH, marine archaeon. This strategy appears to regulate**
20 **membrane homeostasis is common across GDGT-producing lineages, demonstrating that**
21 **diverse taxa adjust membrane composition in response to chronic energy stress.**

22 **Summary**

23
24 **Microorganisms regulate the composition of their membranes in response to environmental**
25 **cues. Many archaea maintain the fluidity and permeability of their membranes by adjusting**
26 **the number of cyclic moieties within the cores of their glycerol dibiphytanyl glycerol**
27 **tetraether (GDGT) lipids. Cyclized GDGTs increase membrane packing and stability, which**
28 **has been shown to help cells survive shifts in temperature and pH. However, the extent of**
29 **this cyclization also varies with growth phase and electron acceptor or donor limitation.**
30 **These observations indicate a relationship between energy metabolism and membrane**
31 **composition. Here we show that the average degree of GDGT cyclization increases with**

32 **doubling time in continuous cultures of the thermoacidophile *Sulfolobus acidocaldarius***
33 **(DSM 639). This is consistent with the behavior of a mesoneutrophile, *Nitrosopumilus***
34 ***maritimus* SCM1. Together, these results demonstrate that archaeal GDGT distributions can**
35 **shift in response to electron donor flux and energy availability, independent of pH or**
36 **temperature. Paleoenvironmental reconstructions based on GDGTs thus capture the energy**
37 **available to microbes, which encompasses fluctuations in temperature and pH, as well as**
38 **electron donor and acceptor availability. The ability of Archaea to adjust membrane**
39 **composition and packing may be an important strategy that enables survival during episodes**
40 **of energy stress.**

41

42 **INTRODUCTION**

43

44 Membrane lipids synthesized by microbes from the domain Archaea can be preserved in
45 sediments for millions of years and are used to reconstruct past environmental conditions.
46 Isoprenoid lipids known as GDGTs (glycerol dibiphytanyl glycerol tetraethers) are the main
47 constituents of mono-layer membranes in many archaea (Kates, 1993; Koga and Morii, 2007).
48 These membrane-spanning lipids and can contain up to eight cyclopentane rings in Cren- and
49 Euryarchaeota, or up to four cyclopentane rings with an additional cyclohexane ring in
50 Thaumarchaeota (Sinninghe Damsté *et al.*, 2002) (Figure S1). These ring structures enhance lipid-
51 lipid interactions (Gabriel and Chong, 2000; Nicolas, 2005; Shinoda *et al.*, 2007a; Shinoda *et al.*,
52 2007b; Pineda De Castro *et al.*, 2016), and ultimately, the packing and stability of the membrane.
53 The relative abundance of these ring structures in GDGTs forms the basis for the widely applied
54 sea- (Schouten *et al.*, 2002; Schouten *et al.*, 2007) and lake- (Powers *et al.*, 2010; Pearson *et al.*,
55 2011) surface paleotemperature proxy known as TEX₈₆.

56 Membrane-spanning tetraether lipids are the most abundant lipids in many thermophilic
57 archaea (Siliakus *et al.*, 2017) and can make up close to 100% of the membranes of acidophilic
58 archaea (Macalady *et al.*, 2004; Oger and Cario, 2013). GDGTs were first identified in
59 hyperthermophilic archaea isolated from hot springs with average temperatures > 60°C; these
60 lipids were originally interpreted as a primary adaptive feature to high temperatures (De Rosa *et al.*
61 *et al.*, 1974). Pure culture experiments with thermoacidophilic crenarchaeota show that the number
62 of pentacyclic rings in the biphytanyl chains of GDGTs increases systematically with growth

63 temperature (De Rosa *et al.*, 1980; Uda *et al.*, 2001; Uda *et al.*, 2004). High temperature, however,
64 is not the only challenge to hot spring microbes. Ecosystems that host thermophiles are often
65 characterized by acidity, and archaeal tetraether-based membranes have also been demonstrated
66 to confer tolerance to low pH (Macalady *et al.*, 2004; Boyd *et al.*, 2013). Archaeal membranes
67 composed of tetraethers are relatively impermeable and thus restrict proton influx into the
68 cytoplasm, allowing cells to better maintain homeostasis at low pH and high temperatures
69 (Elferink *et al.*, 1994; Konings *et al.*, 2002). GDGTs may be linked to the survival of Archaea at
70 these environmental extremes, and calditol-linked GDGTs were recently shown to be required for
71 growth of *Sulfolobus acidocaldarius* under highly acidic conditions (pH < 3) (Zeng *et al.*, 2018).
72 Because these lipids are central to the survival of thermoacidophilic archaea, such organisms are
73 ideal targets to study the role of GDGT cyclization.

74 As a widespread and structurally distinct class of archaeal membrane lipids, GDGTs have
75 been extensively studied with regards to their biophysical properties and role in influencing
76 aggregate membrane behavior. These lipids form stable, highly impermeable monolayers in which
77 individual lipids have low lateral diffusion rates (Jarrel *et al.*, 1998). The incorporation of
78 cyclopentyl rings into these core lipids further increases the thermal stability of membranes.
79 Differential scanning calorimetry experiments on pure lipid films show that thermal transitions are
80 shifted towards higher temperatures as the number of cyclopentane rings increases (Gliozzi *et al.*,
81 1983). The basis for such trends has been illuminated by molecular dynamics simulations across
82 various timescales both *in vacuo* (Gabriel and Chong, 2000) and in solution (Nicolas, 2005;
83 Shinoda *et al.*, 2007a; Shinoda *et al.*, 2007b; Pineda De Castro *et al.*, 2016). These computational
84 studies demonstrate that membranes comprised of highly cyclized GDGTs are more tightly packed,
85 largely due to the more favorable hydrogen bonding interactions that result from the incorporation
86 of cycloalkyl moieties (Gabriel and Chong, 2000; Shinoda *et al.*, 2007a). Tight packing causes
87 membranes composed of cyclized tetraether lipids to become more rigid than membranes
88 composed entirely of acyclic GDGTs. The extent of membrane packing exerts control on microbial
89 physiology, as membrane fluidity and permeability directly influence how the cell interacts with
90 its environment. The closer packing of GDGTs with more pentacyclic rings can explain why
91 compositional variations in these lipids are directly linked to gradients in temperature (De Rosa *et al.*
92 *et al.*, 1980; Uda *et al.*, 2001; Uda *et al.*, 2004) and pH (Yamauchi *et al.*, 1993; van de Vossenberg
93 *et al.*, 1998), as well as energy conservation under heat stress (Sollich *et al.*, 2017).

94 The ability to survive low energy availability may be a defining characteristic of archaea
95 (Valentine, 2007). The relative impermeability of archaeal membranes decreases cellular
96 maintenance energy requirements by reducing inadvertent ion diffusion across the cell membrane
97 (Konings *et al.*, 2002; Hulbert and Else, 2005), implying that the capacity to vary GDGT
98 composition might be an adaptive response to energy limitation. As recently proposed for
99 mesophilic Thaumarchaeota (Hurley *et al.*, 2016), if GDGTs indeed play a role in energy
100 conservation, limiting the energy flux necessary for growth should result in a measurable effect on
101 core GDGT cyclization. We hypothesize this extends to all GDGT-producing archaea, and assess
102 this in a model thermoacidophilic archaeon. In this study we test the effect of limited electron-
103 donor flux on GDGT cyclization in continuous culture (chemostat, Figure S2) experiments with
104 the heterotrophic thermoacidophile *Sulfolobus acidocaldarius* DSM 639. We restrict feed rates of
105 a limiting substrate, sucrose, which acts as both the sole carbon source and electron donor. This
106 strategy allows us to set the specific growth rate of the microbial population while maintaining
107 constant temperature, pH, dissolved oxygen, and chemical composition of the growth medium
108 (Novick and Szilard, 1950; Herbert *et al.*, 1956). This is the first application of continuous culture
109 work to investigate the effects of energy availability on the lipid composition of a
110 thermoacidophilic archaeon. Our chemostat-based approach pares away the confounding variables
111 associated with batch (De Rosa *et al.*, 1980; Uda *et al.*, 2001; Uda *et al.*, 2004, Elling *et al.*, 2014;
112 Elling *et al.*, 2015; Qin *et al.*, 2015; Feyhl-Buska *et al.*, 2016) and mesocosm (Wuchter *et al.*, 2004;
113 Schouten *et al.*, 2007) studies, in which metabolic activity and chemical composition change over
114 the course of the experiment and potentially influence lipid distributions.

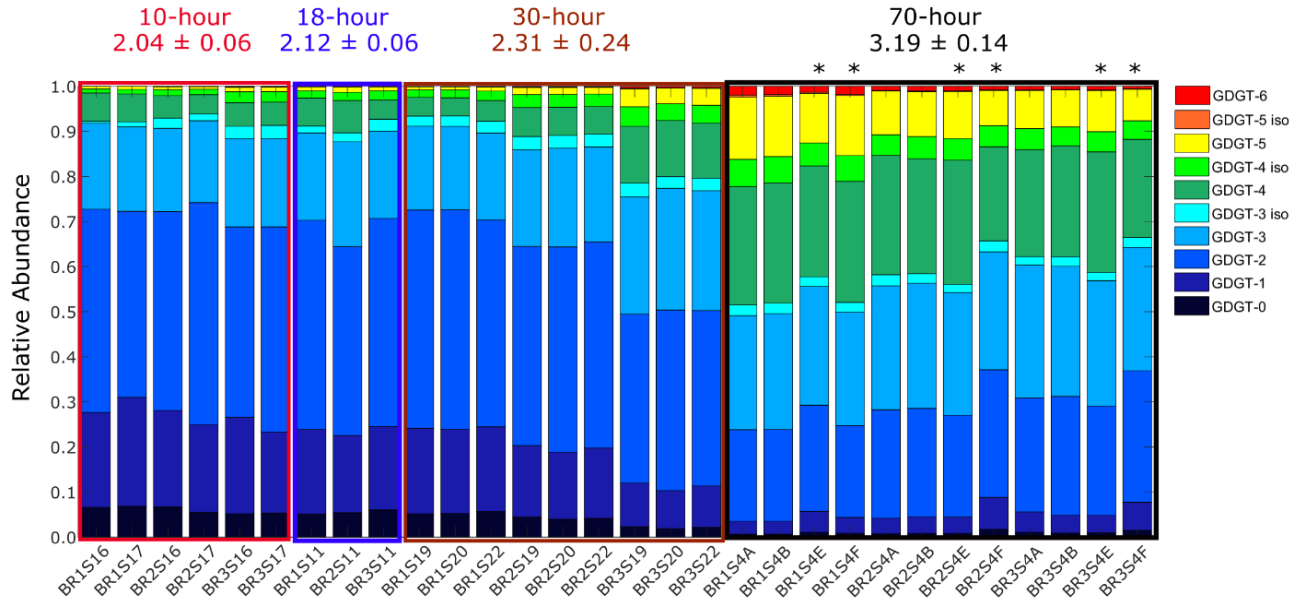
115

116 **RESULTS**

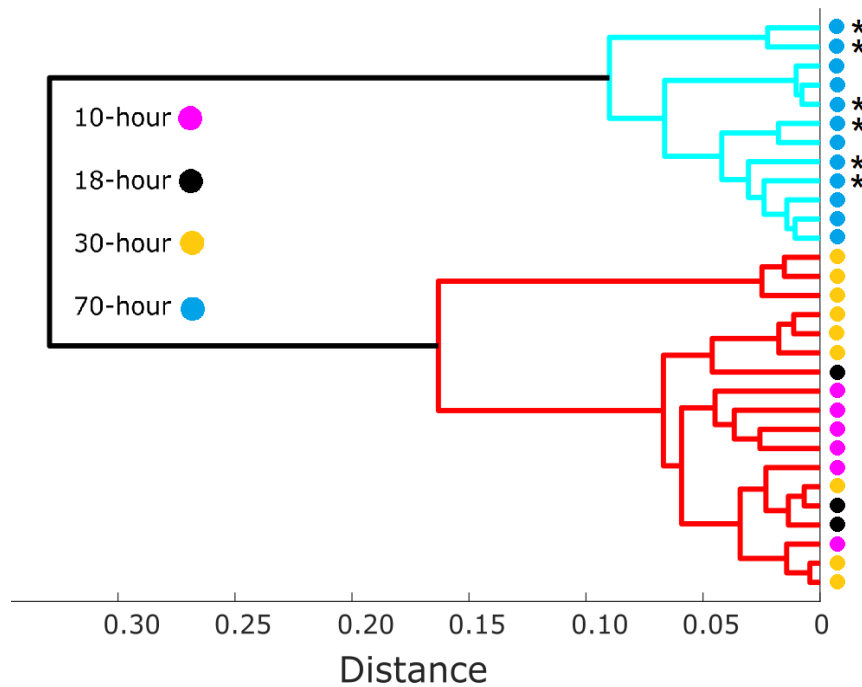
117 **Lipid distributions and ring indices change in response to electron donor supply**

119 Continuous cultures of the crenarchaeon *S. acidocaldarius* produced GDGTs 0-6 at all
120 growth rates, with the average cyclization (expressed as the Ring Index – RI, *see* Methods)
121 increasing at longer doubling times (Figure 1). We observed substantial shifts in the relative
122 abundance of GDGTs with different amounts of cyclopentyl moieties depending on the steady-
123 state growth rates of the cultures (Figure 1). The mean RI changed from 2.04 ± 0.06 at the fastest
124 growth rate to 3.19 ± 0.14 at the slowest growth rate (Figure 1), corresponding to target turnover
125 rates of 9 to 70 h (see Table 1) and inferred doubling times of 7 to 53 h. Changes in RI were caused

126 by shifts in GDGT distributions, as the relative proportion of GDGTs- 4, 5, and 6 increased at
127 slower growth rates (Figure 1). The RI at each target turnover rate (Table 1) was significantly
128 different from all other rates at a 90% confidence level (two-sample *t*-test, $p < 0.02$), except those
129 targets between and 18h and 30h (Figures 2, S2, S4). To test whether collecting biomass over
130 prolonged intervals altered lipid distributions, a direct comparison between cold trap recovery
131 versus instantaneous reactor biomass was carried out in the slowest target turnover rate (70h).
132 Neither GDGT distributions nor RI values differed significantly between biomass collected into
133 cold traps versus biomass sampled directly from bioreactors (Figures 2, S2, S4). Overall, GDGTs
134 were more cyclized at slower reactor turnover times and slower specific growth rates, resulting in
135 higher RI values (Figure 3, S5).
136



138 **Figure 1.** Relative abundances of core GDGTs change solely as a function of doubling time,
139 which we controlled by fixing the provision rate of sucrose to three independent bioreactors (BR1,
140 BR2, BR3). At slower growth rates, lipid distributions are shifted towards more highly cyclized
141 GDGTs-4, 5, and 6. The mean and standard deviations for ring index were averaged across all
142 bioreactors for each target turnover rate, noted above the bar chart. Samples denoted with an
143 asterisk (*) were removed directly from reactors; all other samples were generated from biomass
144 collected into ice-chilled reservoirs.



145

146 **Figure 2.** Average linkage dendrogram (cophenetic correlation coefficient = 0.94) showing
 147 dissimilarities between normalized GDGT distributions measured in samples collected from
 148 cultures spanning 10h to 70h target turnover rate (n = 3). Asterisks (*) are as in Fig. 1.

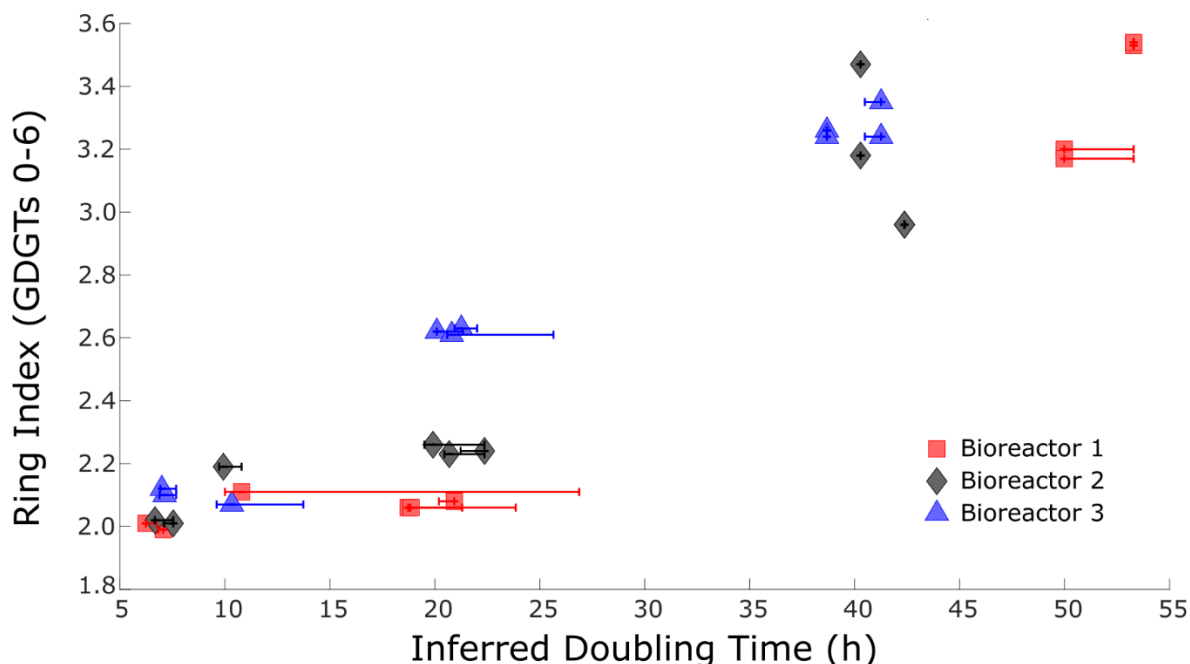
149

150

151 **Table 1.** Target and mean turnover times for the four dilution rate experiments, as well as the associated
 152 inferred population doubling times at steady state. Values account for small volume changes over the
 153 course of the experiment. Intervals in which pumping was interrupted are not included.

Target turnover time (h)	Measured turnover time (h)			Inferred doubling time (h)		
	BR 1	BR 2	BR 3	BR 1	BR 2	BR 3
10	9.2 ± 0.7	9.9 ± 0.4	10.2 ± 0.9	6.9 ± 0.7	7.1 ± 0.9	7.0 ± 0.8
18	17.4 ± 2.3	18.5 ± 3.4	18.0 ± 4.2	12.4 ± 2.1	12.2 ± 2.1	11.9 ± 3.7
30	29.6 ± 0.4	29.9 ± 0.7	31.0 ± 1.6	21.3 ± 4.8	20.4 ± 1.8	21.3 ± 1.4
70	70.2 ± 8.7	62.2 ± 4.6	57.9 ± 4.2	51.6 ± 1.9	41.3 ± 1.2	40.0 ± 1.4

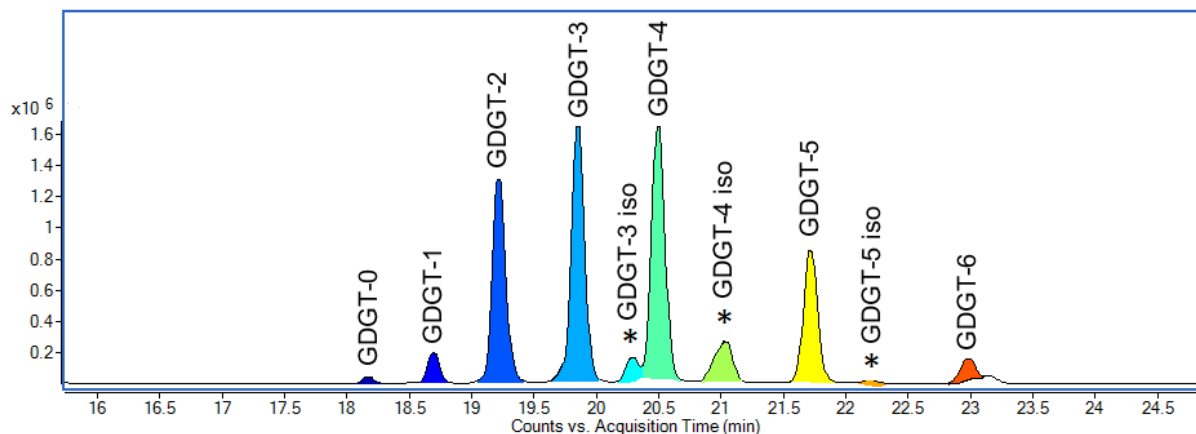
154



155
156 **Figure 3.** Core GDGT cyclization increased systematically as a function of doubling times in
157 isothermal continuous cultures of *S. acidocaldarius*. Growth rates are controlled by restricting flux
158 of the limiting substrate (sucrose, which serves as both the sole carbon and electron source). X-
159 axis error bars represent the maximum range in inferred doubling times observed during the five
160 reactor turnovers preceding each sampling event.

161
162 **Late-eluting GDGT isomers**
163 Small amounts of late-eluting isomers of GDGTs-3, -4, and -5 were observed in all samples
164 (Figures 4 and S6). These molecules are distinct from the early-eluting isomer of GDGT-4
165 characterized in previous studies (Sinninghe Damsté *et al.*, 2012), but may correspond to minor
166 peaks of putative structural isomers observed in *Sulfolobus solfataricus* GDGTs (Hopmans *et al.*,
167 2000). The exact structure of these late-eluting isomers remains unknown. Here we identified them
168 based on their retention times and molecular masses in relation to the major GDGTs (Figure S6).
169 We have also observed these late-eluting GDGT isomers in recent batch experiments with *S.*
170 *acidocaldarius* when the organism was cultivated at conditions associated with the greatest
171 physiological stress, e.g. the highest temperature (80°C) and lowest pH (2.0) tested (data not
172 shown). In this study, the low pH (2.25) may likewise be driving production of late-eluting GDGT
173 isomers. The relative abundances of these isomers were consistent across the entire range of

174 dilution rates tested, which implies that they are not directly involved in a physiological response
175 to energy stress.



176
177 **Figure 4.** A representative base peak chromatogram of *Sulfolobus acidocaldarius* core GDGTs,
178 obtained through high-performance liquid chromatography/atmospheric pressure chemical
179 ionization mass spectrometry (HPLC/APCI-MS), showing the positions and peak heights of late-
180 eluting isomers (*) relative to major isomers.

181

182 DISCUSSION

183
184 Ring index is a measure of the average number of cyclopentane rings within an ensemble
185 of GDGTs. Early laboratory work established an empirical relationship between growth
186 temperature and GDGT cyclization in thermoacidophilic Crenarchaeota (De Rosa *et al.*, 1980; Uda
187 *et al.*, 2001; Uda *et al.*, 2004). Liposome experiments and biophysical models demonstrate that
188 this cyclization is associated with an increase in the degree of membrane packing and a coincident
189 decrease in permeability (Jarrel *et al.*, 1998; Gabriel and Chong, 2000; Nicolas, 2005; Shinoda *et*
190 *al.*, 2007a; Shinoda *et al.*, 2007b; Pineda De Castro *et al.*, 2016). While RI is a useful summary
191 metric of archaeal GDGT profiles, it provides a non-unique description of a lipid ensemble. For
192 example, a pure GDGT-3 membrane would have the same RI (3.0) as a membrane that is 50%
193 GDGT-1 and 50% GDGT-5. It is unknown whether membranes composed of those example lipid
194 populations would have identical biophysical properties. As such, it may be an oversimplification
195 to draw conclusions based solely on RI values.

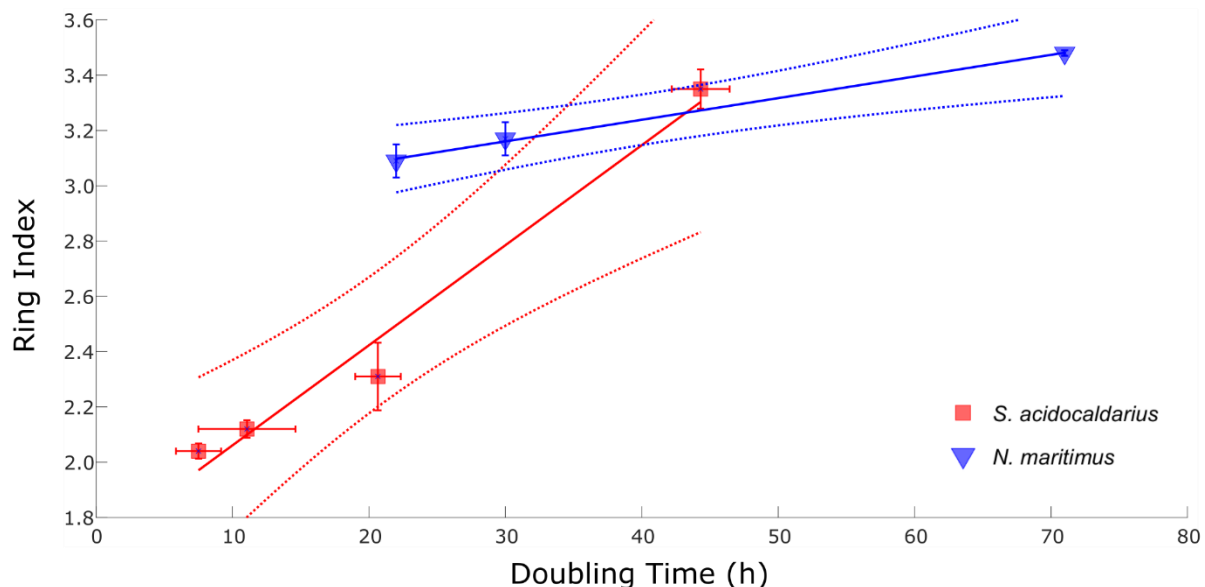
196 The TEX₈₆ ratio is a similar metric that applies to GDGTs produced by marine
197 Thaumarchaeota and is also assumed to be driven by changes in growth temperature (Schouten *et*
198 *al.*, 2002). However, recent pure culture experiments with Thaumarchaeota and Crenarchaeota

199 have shown that other factors significantly alter GDGT distributions, TEX₈₆, and RI. Both
200 mesophilic Thaumarchaeota and thermo(acido)philic Crenarchaeota appear to use GDGT
201 cyclization to regulate membrane permeability and fluidity in response to a number of
202 environmental stressors (Uda *et al.*, 2001; Macalady *et al.*, 2004; Uda *et al.*, 2004; Elling *et al.*,
203 2014; Elling *et al.*, 2015; Qin *et al.*, 2015; Siliakus *et al.*, 2017). Specifically, increases in RI during
204 later growth phases in both Crenarchaeota and Thaumarchaeota (Elling *et al.*, 2014; Jensen *et al.*,
205 2015; Feyhl-Buska *et al.*, 2016), and at reduced O₂ concentrations in experiments with
206 Thaumarchaeota (Qin *et al.*, 2015), suggest that energy conservation is important in influencing
207 archaeal membrane composition. Since nutrient depletion during later growth phases (in batch
208 cultures) and lower dissolved oxygen results in decreased rates of energy supply, these
209 experiments suggest that there may be a direct feedback between energy availability and cellular
210 membrane composition in GDGT-producing Archaea.

211 One means to reduce cellular maintenance energy requirements, regardless of surrounding
212 environmental conditions, is to decrease ion permeability across the cytoplasmic membrane
213 (Valentine, 2007). Maintaining a chemiosmotic potential across the membrane is a significant
214 energy expenditure for all living cells, and the spontaneous diffusion of ions across the membrane
215 not through controlled channels (e.g. ATP synthase) is a form of futile ion cycling and imparts a
216 direct energy loss (Hulbert and Else, 2005; Oger and Cario, 2013). More compact membranes
217 decrease the rate at which ion leakage across the membrane can occur, which will lower cellular
218 maintenance energy requirements. Consistent with this idea, RI should increase at lower energy
219 flux, reflecting an increase in membrane packing under energy limitation. Conversely, RI should
220 decrease as energy availability increases, as the cells would tolerate greater ion leakage. The
221 significant increase in the relative abundance of highly cyclized GDGTs at the slowest sucrose
222 supply rate (Figure 3) supports the hypothesis that tighter membrane packing is a response to
223 energy limitation and may indicate a physiological response to low-power environments (c.f.
224 Bradley *et al.*, 2018).

225 Clear parallels can be drawn between this study and work with another archaeal taxon.
226 Hurley et al. conducted isothermal continuous culture experiments with the mesophilic marine
227 thaumarchaeon *Nitrosopumilus maritimus* SCM1, controlling growth rate by limiting influx of the
228 electron donor, ammonia (Hurley *et al.*, 2016). *N. maritimus* is an ammonia oxidizer of direct
229 relevance to the TEX₈₆ paleotemperature proxy, and the chemostat-based approach used by Hurley

230 et al. constitutes the closest experimental analog to this study. Although *S. acidocaldarius* and *N.*
231 *maritimus* occupy thermally ($T > 60\text{ }^{\circ}\text{C}$ vs. $T < 30\text{ }^{\circ}\text{C}$) and chemically ($\text{pH} < 3$ vs. $\text{pH} > 7$) disparate
232 environments and utilize different carbon and energy metabolisms, they both show a positive
233 correlation between specific growth rate and ring index (Figure 5). For both taxa, RI increased
234 with doubling time (Figure 5), although the relative change in average cyclization between end-
235 member growth rates is more pronounced in *S. acidocaldarius* ($m = 0.036$) than in *N. maritimus*
236 ($m = 0.008$). This agreement implies that membrane dynamics and cellular bioenergetics are tightly
237 coupled in archaea.



238
239 **Figure 5.** Continuous culture experiments plotting doubling time versus ring index from *S.*
240 *acidocaldarius* ($R^2 = 0.98$; $p = 0.01$; $m = 0.036$) relative to *N. maritimus* ($R^2 = 0.99$, $p = 0.03$; $m =$
241 0.008) in Hurley et al. (2016). Data from *S. acidocaldarius* are averaged across triplicate
242 bioreactors for each growth rate versus a single reactor for *N. maritimus*. Dashed lines represent
243 95% confidence intervals.
244

245 A mechanistic understanding of how Archaea regulate GDGT distributions is still lacking
246 due to a limited understanding of the GDGT biosynthesis pathway (42). The synthesis of GDGT
247 core lipids involves the highly unsaturated intermediate, di-geranylgeranyl glycerol phosphate
248 (DGGGP). Formation of GDGT-0 from two molecules of DGGGP requires donation of 28
249 electrons ($14 e^-$ pairs), perhaps via geranylgeranyl reductase, (GGR) (Nishimura and Eguchi, 2006;
250 Sasaki et al., 2011; Jain et al., 2014). Each ring formed reduces this demand by two electrons,
251 providing a direct physiological link between available energy, the formation of cyclopentyl rings,
252 and thus archaeal membrane lipid composition. The synthesis of ring-containing GDGTs also

253 yields the beneficial outcome of decreased ion permeability. This mechanistic idea explains why
254 cyclization of GDGTs varies with specific growth rate even when temperature and pH are held
255 constant, providing a unifying principle to the environmental factors (temperature, pH, dissolved
256 oxygen) that are observationally correlated with changes in archaeal membrane composition (De
257 Rosa *et al.*, 1980; Gliozzi *et al.*, 1983; van de Vossenberg *et al.*, 1998; Uda *et al.*, 2001; Uda *et al.*,
258 2004, Boyd *et al.*, 2013; Elling *et al.*, 2015; Siliakus *et al.*, 2017; Sollich *et al.*, 2017).

259 Changes in GDGT cyclization are more directly quantified by RI than by the TEX₈₆ ratio.
260 RI gives the average number of rings of an entire GDGT pool, whereas TEX₈₆ expresses the
261 abundance of GDGT-1 relative to the other cyclized GDGTs and was developed specifically to
262 relate lipid distributions to sea surface temperatures (Schouten *et al.*, 2002; Schouten *et al.*, 2007).
263 Ideally, both RI and TEX₈₆ would be reported in environmental calibrations or temperature
264 reconstructions, given experimental evidence demonstrating that other factors independently
265 influence GDGT cyclization (Macalady *et al.*, 2004; Elling *et al.*, 2014; Elling *et al.*, 2015; Qin *et*
266 *al.*, 2015; Feyhl-Buska *et al.*, 2016; Hurley *et al.*, 2016). Preliminary work on the utility of RI as
267 a complementary metric shows that coupling it with TEX₈₆ can highlight when GDGT
268 distributions are influenced by non-thermal factors or are behaving differently from average,
269 modern marine communities (Zhang *et al.*, 2016). As expected, RI and TEX₈₆ are significantly
270 correlated; deviations of these indices from the modern TEX₈₆-RI relationship appear to occur
271 when the GDGT signal is overprinted by the effects of variables that do not predominantly
272 correlate with ocean temperature (Zhang *et al.*, 2016).

273 Current calibration functions of the TEX₈₆ paleotemperature proxy systematically
274 underestimate local SSTs in the tropics and overestimate them at the poles (Tierney, 2014). Given
275 the results of this study and previous work documenting the effect of energy availability on RI and
276 TEX₈₆ (Elling *et al.*, 2014; Qin *et al.*, 2015; Hurley *et al.*, 2016), we argue that these biases are
277 likely introduced by temperature-independent environmental and ecological parameters. Marine
278 Thaumarchaeota are ammonia oxidizers whose energy generation is dependent on oxygen as the
279 terminal electron acceptor (Spang *et al.*, 2010; Stahl, D.A. and de la Torre, J.R., 2012). Persistent
280 suboxia and anoxia are common features of modern and ancient restricted basins, such as the proto-
281 Atlantic Ocean during the Cretaceous and Jurassic Oceanic Anoxic Events (Meyer and Kump,
282 2008). These environmental conditions may directly affect the metabolic activity of marine
283 archaea and therefore impact the TEX₈₆ signal in these regions and time intervals. For example,

284 experiments have shown that restricting O₂ supply in batch cultures can result in as much as a
285 10°C increase in TEX₈₆ temperature estimates in excess of experimental incubation temperature
286 (Qin *et al.*, 2015), and a similar shift of 6°C can be induced by altering the electron donor
287 (ammonia) supply in chemostat cultures (Hurley *et al.*, 2016). When the results from both distinct
288 experimental approaches are normalized to the same reference frame, biases in TEX₈₆ are
289 explained by changes in growth rate and ammonia oxidation rate (Hurley *et al.*, 2016). The impact
290 of energy availability on GDGT distributions is therefore important for interpreting sedimentary
291 records from environments influenced by low O₂ concentrations or limited electron-donor
292 availability.

293 Energy limitation may also explain why TEX₈₆-inferred temperatures are anomalously
294 warm (up to +12°C) in modern suboxic settings such as in the permanent oxygen minimum zones
295 (OMZs) of the Eastern Tropical North Pacific Ocean and Arabian Sea, or in seasonally oxygen-
296 deficient regions in coastal upwelling regimes (Basse *et al.*, 2014; Xie *et al.*, 2014; Schouten *et al.*,
297 2012). In support of this theory, sediments from the Murray Ridge seamount summit, which
298 extends into the Arabian Sea OMZ, yield higher TEX₈₆ temperatures than sediment from adjacent
299 locations that lie below the OMZ (Lengger *et al.*, 2012). Conversely, high energy availabilities are
300 associated with cold biases both in controlled pure culture experiments (Elling *et al.*, 2014; Hurley
301 *et al.*, 2016) and in natural settings such as high-nutrient upwelling systems (Lee *et al.*, 2016). In
302 such instances, high productivity and remineralization rates cause RI- and TEX₈₆-derived
303 temperatures to drop below measured temperatures (Hurley *et al.*, 2018).

304 Our study establishes that the heterotrophic thermoacidophile *S. acidocaldarius* exhibits a
305 marked membrane-level response to changes in energy availability. These results provide an
306 important experimental counterpart to continuous culture work with the mesophilic and
307 chemoautotrophic archaeon *N. maritimus* (Hurley *et al.*, 2016). In both studies, energy was varied
308 independent of temperature or pH. Together, these experiments suggest that the denser membrane
309 packing associated with core lipid cyclization is an adaptive mechanism that allows diverse
310 GDGT-producing Archaea to cope with energy stress. Quantifying the influence of cellular
311 bioenergetics on archaeal membrane composition may allow for more complete interpretations of
312 GDGT-based records from hot spring, soil, lake, and marine settings. Biomarker-based
313 reconstructions of past environments can be improved by incorporating calibrations that account

314 for local biogeochemical parameters relevant to archaeal energy metabolisms and subsequent
315 membrane reordering.

316 **METHODS**

317

318 **Culturing conditions**

319 *Sulfolobus acidocaldarius* DSM 639 was provided by Dr. S-V Albers (University of
320 Freiburg, Germany), and cultured at 70°C in complete Brock medium supplemented with 0.1%
321 NZ-Amine and 0.2% sucrose (see *SI Materials and Methods*) at pH 2.25 (\pm 0.2). Initial cultures
322 were grown at 70°C and 200 rpm (Innova-42 shaking incubators, Eppendorf). Three 1-L
323 autoclavable glass bioreactors (Applikon, Delft, The Netherlands) were subsequently inoculated
324 with 20 mL of a second-generation culture at mid-exponential phase to an initial optical density of
325 0.01 at 600 nm (OD₆₀₀).

326 The three bioreactors were operated in parallel under continuous culture conditions (see *SI*
327 *Materials and Methods*; Figure S2). Reactors were maintained at 70°C, stirred at 200 rpm
328 (Rushton-type impeller), and aerated with a constant flux of 200 mL/min Zero Air (ultra-high
329 purity, UHP). To reduce evaporative volume loss, excess gas was released through condensers in
330 the reactor headplate. Reactor liquid volume was held constant at 500 mL by equalizing influent
331 and effluent pump rates using a balance control loop (Applikon My-Control software).
332 Temperature, dissolved oxygen, pH, and balance readings were logged continuously using the
333 Lucullus Process Information Management System interface (Applikon).

334 In four consecutive experiments, the flow rate of the influent and effluent medium was set
335 to target four discrete specific growth rates, $\mu = 0.069, 0.039, 0.023, 0.010 \text{ h}^{-1}$, corresponding to
336 reactor turnover times of $T_t = 10, 18, 30, \text{ and } 70 \text{ h}$, respectively. Cell concentrations were
337 monitored by optical density measurements at 600 nm, and coincident fluctuations in dilution rate
338 and optical densities were then used to calculate growth rate and deviation from steady-state.

339

340 **Lipid analysis**

341 Biomass collection was initiated after each bioreactor had operated at or within $\pm 10\%$ of
342 steady state for three consecutive turnovers at a given growth rate (Figures S7 and S8). Following
343 collection of effluent into cold traps placed on ice, four 50 mL aliquots from each trap were
344 centrifuged at 3214 x g and 4°C for 30 minutes (Eppendorf 5810 R, S-4-104 rotor). The
345 supernatant was decanted after centrifugation and cell pellets were stored at -80°C until ready for
346 freeze-drying and lipid extraction. To determine whether prolonged effluent collection impacted
347 lipid distributions, 10 mL aliquots were also pulled directly from bioreactors during all 70 h

348 experiment sampling events. Aliquots were drawn out through a syringe port and then processed
349 as above.

350 Core GDGTs were isolated from freeze-dried biomass by acid hydrolysis followed by
351 ultrasonic solvent extraction (e.g. Weber *et al.*, 2017). To this end, freeze-dried cell pellets
352 representing 50 mL aliquots of cell culture were submerged in 3 N methanolic HCl (33% H₂O) for
353 3 hours at 70 °C. After cooling, methyl-tert-butyl-ether (MTBE) was added to achieve a
354 MTBE:methanol ratio of 1:1 (vol.) and the samples were agitated using a Qsonica Q500 ultrasonic
355 probe (cup horn, maximum amplitude, 5 minutes total pulse time). Phase separation was induced
356 by changing the solvent composition to MTBE:methanol:hexane (1:1:1, vol.), and the upper
357 organic phase was collected after centrifugation. The total lipid extract (TLE) was subsequently
358 dried under a flow of N₂ and stored at -20°C in a solution of 1% isopropyl alcohol (IPA) in hexane
359 until analysis.

360 Core GDGTs were analyzed by ultra-high performance liquid chromatography -
361 atmospheric pressure chemical ionization - mass spectrometry (UHPLC-APCI-MS) using an
362 Agilent 1290 Infinity series UHPLC system coupled to an Agilent 6410 triple-quadrupole mass
363 spectrometer (MS), operated in positive mode (gas temperature: 350 °C; vaporizer temperature:
364 300°C; gas flow: 6 L min⁻¹, nebulizer pressure: 60 psi). Analytical separation of GDGTs was
365 achieved by injecting 2–10 µL of the total lipid extract onto an array of two coupled Acquity BEH
366 HILIC amide columns (2.1 × 150 mm, 1.7 µm particle size, Waters, Eschborn, Germany)
367 maintained at 50°C and fitted with a pre-column of the same material. GDGTs were eluted using
368 a linear gradient from 0.2% to 10% (vol.) IPA in hexane at a flow rate of 0.5 ml/min as previously
369 described (39). At the end of each sample run, the columns were back-flushed with a 70:30 mixture
370 of hexane:IPA (90:10, vol:vol) and IPA:methanol (70:30, vol:vol), and the columns were re-
371 equilibrated to initial condition. The MS was operated in single ion monitoring mode (dwell time
372 25 ms, fragmentor voltage: 75 V) and GDGTs were quantified by integration of the ion
373 chromatograms of m/z 1302.3 (GDGT-0), m/z 1300.3 (GDGT-1), etc. The ring index (RI) of
374 GDGTs reflects the relative amount of cyclopentyl rings and is defined as:

375

$$376 \quad \text{RI} = \frac{1x[\text{GDGT-1}] + 2x[\text{GDGT-2}] + 3x[\text{GDGT-3}] + 4x[\text{GDGT-4}] + 5x[\text{GDGT-5}] + 6x[\text{GDGT-6}]}{[\text{GDGT-0}] + [\text{GDGT-1}] + [\text{GDGT-2}] + [\text{GDGT-3}] + [\text{GDGT-4}] + [\text{GDGT-5}] + [\text{GDGT-6}]} \quad (1)$$

377

378 The RI metric compresses GDGT distributions into a single value representing the average number
379 of cyclopentyl rings in GDGTs for each sample.

380

381 **Growth rate and doubling time calculations**

382 Cell densities were monitored at regular intervals throughout the experiment by measuring
383 the absorbance at 600 nm (A600) of a 1 mL aliquot pulled directly from each bioreactor. Dilution
384 rates and turnover times were calculated by measuring the volume of effluent pumped out of each
385 reactor per collection interval.

386 The net rate of change in cell concentration (dx/dt) is a function of the rates of cell division and
387 dilution by sterile medium:

$$388 \quad dx/dt = \mu x - Dx \quad (2)$$

389 where x = concentration of cells, μ = specific growth rate of the organism, and D = dilution rate
390 (Novick and Szilard, 1950; Herbert *et al.*, 1956). At steady state, the population's specific growth
391 rate (μ) is equal to the dilution rate (D), such that the concentration of cells does not change with
392 time ($dx/dt = 0$). Deviation from theoretical steady-state are approximated by calculating the
393 difference between μ and D . Dilution rate is determined by measuring the rate of liquid effluent
394 outflow, and μ is then estimated from measured absorbance data using a rearranged form of
395 Equation 2:

$$396 \quad \mu = \frac{\frac{dx}{dt} + Dx}{x} \quad (3)$$

397 Here dx/dt is the change in A600 between two consecutive time points (i.e. $\Delta A600/\Delta t$, in h^{-1}), D
398 is calculated dilution rate (h^{-1}) over the time interval, and x is the measured A600 value at given
399 time point. The value of μ then used to calculate doubling time:

$$400 \quad \text{Doubling time} = \frac{\ln(2)}{\mu} \quad (4)$$

401 We control and measure both dilution rate and reactor turnover time along with the
402 corresponding biologically relevant metrics, i.e. the calculated specific growth rate and doubling
403 time. At a theoretical steady state in a chemostat, the specific growth rate of a population exactly
404 equals the reactor dilution rate: $\mu = D$. In practice, however, small variances between μ and D can
405 emerge due to the dynamical nature of the reactor system and/or the microbial populations.
406 Deviations from steady state may be driven by transient fluctuations in the internal state of

407 microorganisms, the delivery rate of nutrients, or both. The deviation from theoretical steady-state
408 is expressed in relative terms as:

409
$$\text{Deviation from steady-state (\%)} = \frac{\mu - D}{D} \times 100\%. \quad (5)$$

410 Percent deviation from an idealized steady-state was calculated and recorded each time optical
411 density measurements were taken.

412

413 **Statistical analysis**

414 A two-sample *t*-test was used to assess whether the mean RI associated with each growth
415 rate is significantly different from the others (Figure S4). In order to compare the relative
416 abundances of core GDGT variants between samples, we computed a Euclidian distance matrix
417 and visualized dissimilarities between samples by hierarchical clustering using an average linkage
418 technique (Figure S3). All statistical analysis was carried out in MATLAB R2019b; scripts and
419 data files are available online at [https://github.com/AliceZhou73/Chemostat-Paper---Code-and-](https://github.com/AliceZhou73/Chemostat-Paper---Code-and-Data-Files)
420 [Data-Files](https://github.com/AliceZhou73/Chemostat-Paper---Code-and-Data-Files).

421

422

423 **Acknowledgements**

424 For financial support we thank the ACS-PRF DNI #57209-DNI2 (WDL/YW), the Walter &
425 Constance Burke Fund at Dartmouth College (WDL) and the NASA award NNX15AH79H; Swiss
426 National Science Foundation (YW); and the Gordon and Betty Moore Foundation and NSF-
427 1702262 (AP/FJE). We thank the other members of the Leavitt and Pearson labs for thoughtful
428 discussion and support.

429

430 **Supplemental Data**

431

432 *Code:* <https://github.com/AliceZhou73/Chemostat-Paper---Code-and-Data-Files>

433 *Supplementary Information:* Temporary Link: <https://figshare.com/s/a8a430482f6e3300c99c>

434

435

436 **References**

- 437
- 438 Basse, A., Zhu, C., Versteegh, G.J.M, Fischer, G., Hinrichs, K-W., and Mollenhauer, G. (2014) Distribution
439 of intact and core tetraether lipids in water column profiles of suspended particulate matter off Cape Blanc,
440 NW Africa. *Organic Geochemistry* **72**: 1-13.
- 441
- 442 Bradley, J.A., Amend, J.P., and LaRowe, D.E. (2018) Bioenergetic controls on microbial ecophysiology in
443 marine sediments. *Frontiers in Microbiology* **9**: 180.
- 444
- 445 Becker, K.W., Lipp, J.S., Zhu, C., Liu, X-L., and Hinrichs, K-U. (2013) An improved method for the
446 analysis of archaeal and bacterial ether core lipids. *Organic Geochemistry* **61**: 34-44.
- 447
- 448 Boyd, E.S., Hamilton, T.L., Wang, J., He, L., and Zhang, C.L. (2013) The role of tetraether lipid
449 composition in the adaptation of thermophilic archaea to acidity. *Frontiers in Microbiology* **4**: 62.
- 450
- 451 de Rosa, M., Gambacorta, A., Minale, L., and Bu'Lock, J. (1974) Cyclic diether lipids from very
452 thermophilic acidophilic bacteria. *Journal of the Chemical Society, Chemical Communications* **14**: 543-
453 544.
- 454
- 455 de Rosa, M., Esposito, E., Gambacorta, A., Nicolaus, B., and Bu'Lock, J.D. (1980) Effects of temperature
456 on ether lipid composition of *Caldariella acidophila*. *Phytochemistry* **19(5)**: 827-831.
- 457
- 458 Elferink, M.G., de Wit, J.G., Driessen, A.J., and Konings, W.N. (1994) Stability and proton-permeability
459 of liposomes composed of archaeal tetraether lipids. *Biochimica et Biophysica Acta* **1193(2)**: 247-254.
- 460
- 461 Elling, F.J., et al. (2014) Effects of growth phase on the membrane lipid composition of the thaumarchaeon
462 *Nitrosopumilus maritimus* and their implications for archaeal lipid distributions in the marine environment.
463 *Geochimica et Cosmochimica Acta* **141**: 579-597.
- 464
- 465 Elling, F.J., Könneke, M., Mußmann, M., Greve, A., and Hinrichs, K-U. (2015) Influence of temperature,
466 pH, and salinity on membrane lipid composition and TEX₈₆ of marine planktonic thaumarchaeal isolates.
467 *Geochimica et Cosmochim Acta* **171**: 238-255.
- 468
- 469 Feyhl-Buska, J., Chen, Y., Jia, C., Wang, J-X., Zhang, C.L., and Boyd, E.S. (2016) Influence of growth
470 phase, pH, and temperature on the abundance and composition of tetraether lipids in the thermoacidophile
471 *P. torridus*. *Frontiers in Microbiology* **7**: 1332.
- 472
- 473 Gabriel, J.L. and Chong, P.L.G. (2000) Molecular modeling of archaeobacterial bipolar tetraether lipid
474 membranes. *Chemistry and Physics of Lipids* **105**: 193-200.
- 475
- 476 Gliozzi, A., Paoli, G., De Rosa, M., and Gambacorta, A. (1983) Effect of isoprenoid cyclization on the
477 transition temperature of lipids in thermophilic archaeobacteria. *Biochimica et Biophysica Acta* **735**: 234-
478 242.
- 479
- 480 Herbert, D., Elsworth, R., and Telling, R.C. (1956) The continuous culture of bacteria; a theoretical and
481 experimental study. *Journal of General Microbiology* **14**: 601-622.
- 482
- 483 Hopmans, E.C., Schouten, S., Pancost, R.D., van der Meer, M.T.J., and Sinninghe-Damsté, J.S. (2000)
484 Analysis of intact tetraether lipids in archaeal cell material and sediments by high performance liquid

- 485 chromatography/atmospheric pressure chemical ionization mass spectrometry. *Rapid Communications in*
486 *Mass Spectrometry* **14**: 585-589.
- 487
- 488 Hulbert, A.J. and Else, P.L. (2005) Membranes and the setting of energy demand. *Journal of Experimental*
489 *Biology* **208**: 1593–1599.
- 490
- 491 Hurley, S.J., Elling, F.J., Könneke, M., Buchwald, C., Wankel, S.D., Santoro, A.E., Lipp, J.S., Hinrichs, K-
492 U., and Pearson, A. (2016) Influence of ammonia oxidation rate on thaumarchaeal lipid composition and
493 the TEX₈₆ temperature proxy. *Proceedings of the National Academy of Sciences* **113**(28): 7762-7677.
- 494
- 495 Hurley, S.J., Lipp, J.S., Close, H.G., Hinrichs, K-U., and Pearson, A. (2018) Distribution and export of
496 isoprenoid tetraether lipids in suspended particulate matter from the water column of the Western Atlantic
497 Ocean. *Organic Geochemistry* **116**: 90-102.
- 498 Jain, S., Caforio, A., and Driessen, A.J.M. (2014) Biosynthesis of archaeal membrane ether lipids. *Frontiers*
499 *in Microbiology* **5**: 641.
- 500
- 501 Jarrel, H.C., Zukotynski, K.A., and Sprott, G.D. (1998) Lateral diffusion of the total polar lipids from
502 *Thermoplasma acidophilum* in multilamellar liposomes. *Biochimica et Biophysica Acta - Biomembranes*
503 **1369**(2): 259-266.
- 504
- 505 Jensen, S.M., Neesgaard, V.L., Skjoldbjerg, S.L.N., Brandl, M., Ejsing, C.S., and Treusch, A.H. (2015)
506 The effects of temperature and growth phase on the lipidomes of *Sulfolobus icelandicus* and *Sulfolobus*
507 *tokodaii*. *Life (Basel)* **5**(3): 1539-1566.
- 508
- 509 Kates, M. (1993) The Biochemistry of Archaea (Archaeobacteria). *Membrane Lipids of Archaea*, eds.
510 Kushner DJ, Matheson AT (Elsevier Science, Amsterdam), 261-295.
- 511
- 512 Koga, Y. and Morii, H. (2007) Biosynthesis of ether-type polar lipids in archaea and evolutionary
513 considerations. *Microbiology and Molecular Biology Reviews* **71**: 97-120.
- 514
- 515 Konings, W.N., et al. (2002) The cell membrane plays a crucial role in survival of bacteria and archaea in
516 extreme environments. *Antonie Van Leeuwenhoek* **81**: 61-72.
- 517
- 518 Lee, K.E., Kim, J-H., Wilke, I., Helmke, P., and Schouten, S. (2008) A study of the alkenone, TEX₈₆, and
519 planktonic foraminifera in the Benguela Upwelling System: Implications for past sea surface temperature
520 estimates. *Geochemistry, Geophysics, Geosystems* **9**(10), Q10019,
- 521
- 522 Lengger, S.K., Hopmans, E.C., Reichart, G-J., Nierop, K.G.J., Sinninghe-Damsté, J.S., and Schouten, S.
523 (2012) Intact polar and core glycerol dibiphytanyl glycerol tetraether lipids in the Arabian Sea oxygen
524 minimum zone: II. Selective preservation and degradation in sediments and consequences for the TEX₈₆.
525 *Geochimica et Cosmochimica Acta* **98**: 244-258.
- 526
- 527 Macalady, J.L., Vestling, M.M., Baumler, D., Boekelheide, N., Kaspar, C.W., and Banfield, J.F. (2004)
528 Tetraether-linked membrane monolayers in *Ferroplasma* spp: a key to survival in acid. *Extremophiles* **8**:
529 411-419.
- 530
- 531 Meyer, K.M. and Kump, L.R. (2008) Oceanic euxinia in Earth history: Causes and consequences. *Annual*
532 *Review of Earth and Planetary Sciences* **36**: 251-288.
- 533
- 534 Nicolas, J.P. (2005) A molecular dynamics study of an archaeal tetraether lipid membrane: comparison
535 with a dipalmitoylphosphatidylcholine lipid bilayer. *Lipids* **40**: 1023-1030.

- 536
537 Nishimura Y and Eguchi T (2006). Biosynthesis of archaeal membrane lipids:
538 Digeranylgeranyl glycerophospholipid reductase of the thermoacidophilic archaeon *Thermoplasma*
539 *acidophilum*. *The Journal of Biochemistry* **139**(6): 1073–1081.
540 Novick, A. and Szilard, L. (1950) Description of the chemostat. *Science* **15**;112(2920): 715-716.
541
542 Oger, P.M. and Cario, A. (2013) Adaptation of the membrane in Archaea. *Biophysical Chemistry* **183**: 42-
543 56.
544
545 Pearson, E.J., et al. (2011) A lacustrine GDGT-temperature calibration from the Scandinavian Arctic to
546 Antarctic: Renewed potential for the application of GDGT paleothermometry in lakes. *Geochimica et*
547 *Cosmochimica Acta* **75**: 6225–6238.
548
549 Pineda De Castro, L.F., Dopson, M., and Friedman, R. (2016) Biological membranes in extreme conditions:
550 simulations of anionic archaeal tetraether lipid membranes. *PLoS ONE* **11**(5): e0155287.
551
552 Powers, L., Werne, J.P., Vanderwoude, A.J., Sinninghe Damsté, J.S., Hopmans, E.C., and Schouten, S.
553 (2010) Applicability and calibration of the TEX₈₆ paleothermometer in lakes. *Organic Geochemistry* **41**(4):
554 404–413.
555
556 Qin, W., Carlson, L.T., Armbrust, E.V., Devol, A.H., Moffett, J.W., Stahl, D.A., and Ingalls, A.E. (2015)
557 Confounding effects of oxygen and temperature on the TEX₈₆ signature of marine Thaumarchaeota.
558 *Proceedings of the National Academy of Sciences USA* **112**(35): 10979–10984.
559
560 Sasaki, D., Fujihashi, M., Iwata, Y., Murakami, M., Yoshimura, T., Hemmi, H., and Miki, K. (2011)
561 Structure and mutation analysis of archaeal geranylgeranyl reductase. *Journal of Molecular Biology* **409**(4):
562 543–557.
563
564 Schouten, S., Hopmans, E.C., Schefuß, E., and Sinninghe Damsté, J.S. (2002) Distributional variations in
565 marine crenarchaeotal membrane lipids: a new tool for reconstructing ancient sea water temperatures?
566 *Earth and Planetary Science Letters* **204**: 265-274.
567
568 Schouten, S., Forster, A., Panoto, F.E., and Sinninghe Damsté, J.S. (2007a) Towards calibration of the
569 TEX₈₆ paleothermometer for tropical sea surface temperatures in ancient greenhouse worlds. *Organic*
570 *Geochemistry* **38**: 1537-1546.
571
572 Schouten, S., Hugué, C., Hopmans, E.C., Kienhuis, M.V.M., and Sinninghe Damsté, J.S. (2007b)
573 Analytical methodology for TEX₈₆ paleothermometry by high-performance liquid
574 chromatograph/atmospheric pressure chemical ionization-mass spectrometry. *Analytical Chemistry* **79**(7):
575 2940-2944.
576
577 Schouten, S., Pitcher, A., Hopmans, E.C., Villanueva, L., Bleijswijk, J., and Sinninghe-Damsté, J.S. (2012)
578 Intact polar and core glycerol dibiphytanyl glycerol tetraether lipids in the Arabian Sea oxygen minimum
579 zone: I. Selective preservation and degradation in the water column and consequences for the TEX₈₆.
580 *Geochimica et Cosmochimica Acta* **98**: 228-243.
581
582 Shinoda, K., Shinoda, W., Baba, T., and Mikami, M. (2007) Molecular dynamics study of bipolar tetraether
583 lipid membranes. *Biophysical Journal* **89**: 3195-3202.
584
585 Shinoda, K., Shinoda, W., and Mikami, M. (2007) Molecular dynamics simulation of an archaeal lipid
586 bilayer with sodium chloride. *Physical Chemistry Chemical Physics* **9**(5): 643–650.

587
588 Siliakus, M.F., van der Oost, J., and Kengen, S.W.M. (2017) Adaptations of archaeal and bacterial
589 membranes to variations in temperature, pH and pressure. *Extremophiles* **21**: 651-670.
590
591 Sinninghe Damsté, J.S., Hopmans, E.C., Schouten, S., Van Duin, A.C.T., and Geenevasen, J.A.J. (2002)
592 Crenarchaeol: the characteristic core glycerol dibiphytanyl glycerol tetraether membrane lipid of
593 cosmopolitan pelagic crenarchaeota. *Journal of Lipid Research* **43**: 1641-1651.
594
595 Sinninghe Damsté, J.S., Rijpstra, W.I.C., Hopmans, E.C., Jung, M-Y., Kim, J-G., Rhee, S-K., Stieglmeier,
596 M., and Schleper, C. (2012) Intact polar and core glycerol dibiphytanyl glycerol tetraether lipids of Group
597 I.1a and I.1b Thaumarchaeota in soil. *Applied and Environmental Biology* **78**(19): 6866-6874.
598
599 Spang A, et al. (2010) Distinct gene set in two different lineages of ammonia-oxidizing archaea supports
600 the phylum Thaumarchaeota. *Trends in Microbiology* **18**(8): 331–340.
601
602 Sollich, M., Yoshinaga, M.Y., Häusler, S., Price, R.E., Hinrichs, K-U., and Bühring, S.I. (2017) Heat stress
603 dictates microbial lipid composition along a thermal gradient in marine sediments. *Frontiers in*
604 *Microbiology* **8**: 1550.
605
606 Stahl, D.A. and de la Torre, J.R., (2012). Physiology and diversity of ammonia-oxidizing archaea. *Annual*
607 *review of microbiology*, **66**: 83-101.
608
609 Tierney, J.E. (2014) Biomarker-based inferences of past climate: the TEX₈₆ paleotemperature proxy.
610 *Treatise on Geochemistry: Second Edition*. 12. 379-393.
611
612 Uda, I., Sugai, A., Itoh, Y.H., and Itoh T (2001) Variation in molecular species of polar lipids from
613 *Thermoplasma acidophilum* depends on growth temperature. *Lipids* **36**(1): 103-105.
614
615 Uda, I., Sugai, A., Itoh, Y.H., and Itoh, T. (2004) Variation in molecular species of core lipids from the
616 order *Thermoplasmatales* strains depends on the growth temperature. *Journal of Oleo Science* **53**: 399-404.
617
618 Valentine, D.L. (2007) Adaptations to energy stress dictate the ecology and evolution of the Archaea.
619 *Nature Reviews Microbiology* **5**(4): 316–323.
620
621 van de Vossenberg, J., Driessen, A.J.M., Zillig, W., and Konings, W.N. (1998) Bioenergetics and
622 cytoplasmic membrane stability of the extremely acidophilic, thermophilic archaeon *Picrophilus oshimae*.
623 *Extremophiles* **2**(2): 67-74.
624
625 Weber, Y., Sinninghe Damsté, J.S., Hopmans, E.C., Lehmann, M.F., and Niemann, H. (2017) Incomplete
626 recovery of intact polar glycerol dialkyl glycerol tetraethers from lacustrine suspended biomass. *Limnology*
627 *and Oceanography: Methods* **15**(9): 782–793.
628
629 Wuchter, C., Schouten, S., Coolen, M.J.L., and Sinninghe Damsté, J.S. (2004) Temperature-dependent
630 variation in the distribution of tetraether membrane lipids of marine Crenarchaeota: Implications for TEX₈₆
631 paleothermometry. *Paleoceanography and Paleoclimatology* **19**(4), PA4028.
632
633 Xie, S.T., Liu, X.L., Schubotz, F., Wakeham, S.G., and Hinrichs, K.U. (2014) Distribution of glycerol ether
634 lipids in the oxygen minimum zone of the Eastern Tropical North Pacific Ocean. *Organic Geochemistry*
635 **71**: 60-71.
636

- 637 Yamauchi, K., Doi, K., Yoshida, Y., and Kinoshita, M. (1993) Archaeobacterial lipids: highly proton-
638 impermeable membranes from 1,2-diphytanyl-sn-glycero-3-phosphocholine. *Biochimica et Biophysica*
639 *Acta* **1146**: 178–182.
640
- 641 Zhang, Y.G., Pagani., M., and Wang, Z (2016) Ring index: A new strategy to evaluate the integrity of
642 TEX₈₆ paleothermometry. *Paleoceanography* **31**: 220-232.
643
- 644 Zeng, Z., Liu, X-L., Wei, J.H., Summons, R.E., and Welander, P.V. (2018). Calditol-linked membrane
645 lipids are required for acid tolerance in *Sulfolobus acidocaldarius*. *Proceedings of the National Academy*
646 *of Sciences* **115**(51): 12932-12937.
647

